Published in final edited form as:
Synapse. 2013 August ; 67(8): 515–531. doi:10.1002/syn.21674.

Early Degeneration of Photoreceptor Synapse in *Ccl2/Cx3cr1*-Deficient Mice on *Crb1*^{rd8} Background

Jun Zhang[1,*], **Jingsheng Tuo**[2], **Xiaoguan Cao**[2,3], **Defen Shen**[2], **Wei Li**[4], and **Chi-Chao Chan**[1,2,*]

[1]Histology Core, National Eye Institute, National Institutes of Health, Bethesda, Maryland
[2]Laboratory of Immunology, National Eye Institute, National Institutes of Health, Bethesda, Maryland [3]Department of Ophthalmology, People's Hospital, Peking University, Beijing, China
[4]Unit of Retinal Neurophysiology, National Eye Institute, National Institutes of Health, Bethesda, Maryland

Abstract

Photoreceptor ribbon synapse releases glutamate to postsynaptic targets. The synaptic ribbon may play multiple roles in ribbon synapse development, synaptic vesicle recycling, and synaptic transmission. Age-related macular degeneration (AMD) patients appear to have fewer or no detectable synaptic ribbons as well as abnormal swelling in the photoreceptor terminals in the macula. However, reports on changes of photoreceptor synapses in AMD are scarce and photoreceptor type and quantity affected in early AMD is still unclear. Here, we employed multiple anatomical techniques to investigate these questions in *Ccl2*$^{-/-}$/*Cx3cr1*$^{-/-}$ mouse on *Crb1*^{rd8} background (DKO *rd8*) at one month of age. We found that approximately 17% of photoreceptors over the focal lesion were lost. Immunostaining for synapse-associated proteins (CtBP2, synaptophysin, and vesicular glutamate transporter 1) showed significantly reduced expression and ectopic localization. Cone opsins demonstrated dramatic reduction in expression (S-opsins) and extensive mislocalization (M-opsins). Quantitative ultrastructural analysis confirmed a significant decrease in the number of cone terminals and nuclei, numerous vacuoles in remaining cone terminals, reduction in the number of synaptic ribbons in photoreceptor terminals, and ectopic rod ribbon synapses. In addition, glutamate receptor immunoreactivity on aberrant sprouting of rod bipolar cells and horizontal cells were identified at the ectopic synapses. These results indicate that synaptic alterations occur at the early stages of disease and cones are likely more susceptible to damage caused by DKO *rd8* mutation. They provide a new insight into potential mechanism of vision function lost due to synaptic degeneration before cell death in the early Stages of AMD.

Keywords

age-related macular degeneration; cone synapse degeneration; rod synapse plasticity; animal model

*Correspondence to: Chi-Chao Chan, 10 Center Dr., Bldg. 10, Rm. 10N103, NIH/NEI, Bethesda, MD 20892-1857, USA. chanc@nei.nih.gov or Jun Zhang, 35 Convent Dr., Bldg. 35, Rm. 3C1004, NINDS/NIH, Bethesda, MD 20892 USA. junzhang@ninds.nih.gov.

J.Z. designed the experiments and conducted histology, electron microscopy, immunofluorescence, data analysis, and wrote the article. J.T. reviewed the article. X.C. and D.S. took care of the mice. W.L. and C.-C.C. participated in the design of the experiments, data analyses, and critical review of the manuscript. All authors approved the final article.

INTRODUCTION

Photoreceptors release glutamate, both in tonic or transient fashions, to postsynaptic bipolar cells (BCs) and horizontal cells (HCs) (Sterling and Matthews, 2005). To support these functional requirements, photoreceptor terminals are highly specialized with the presence of synaptic ribbon, which tether numerous synaptic vesicles near the presynaptic release site (Dowling and Boycott, 1966). Synaptic ribbons play multiple roles in ribbon synapse formation, recycling of synaptic vesicles, and synaptic transmission (Matthews and Fuchs, 2010; Regus-Leidig et al., 2010; Sterling and Matthews, 2005; Wan et al., 2005). A study done in zebrafish reported that knockdown of bipolar cellular ribeye, the main component of synaptic ribbon, resulted in the disappearance of synaptic ribbons (Wan et al., 2005). Additionally, functional deletion of bassoon, a cytomatrix protein associated with ribbon, causing disassociation of ribbon from the active zone, led to impaired photoreceptor synaptic transmission and ectopic synapse formation in mutant mice (Dick et al., 2003; Regus-Leidig et al., 2010; tom Dieck et al., 2005). Thus, investigating ribbon synapse formation and maintenance is important for better understanding of visual signal transmission in physiological conditions and in many retinal diseases, including those of retinal degeneration.

CCL2, a CC chemokine and released from retinal glia, binds to CCR2 receptor to mediates adhesion of inflammatory cells to vessels (Rutar et al., 2011). Aging *Ccl2*$^{-/-}$ mice were found to have features of age-related macular degeneration (AMD) (Ambati et al., 2003), indicating *Ccl2* plays a key role in AMD pathogenesis (Forrester, 2003). CX3CR1, a receptor for CX3CL1/fractalkine chemokine, is expressed in various immune cells and microglia in the retina (Imai et al., 1997; Niess et al., 2005; Savarin-Vuaillat and Ransohoff, 2007; Sunnemark et al., 2003). We and others have reported that CX3CR1 polymorphisms are associated with AMD and further demonstrated a decreased number of CX3CR1 transcripts and protein in AMD (Anastasopoulos et al, 2012; Chan et al., 2005; Combadière, 2007; Tuo et al., 2004; Yang et al, 2010). *Cx3cr1*-deficient mouse has been reported to develop AMD-like features (Combadière et al., 2007; Raoul et al., 2007). We hypothesized therefore that both *Cx3cr1* and *Ccl2* double deficiency might have a synergistic effect to form a phenotype displaying focal retinal lesions with early onset and high penetrance (Chan et al., 2008; Tuo et al., 2007). As expected, *Ccl2*$^{-/-}$/*Cx3cr1*$^{-/-}$ mouse on *Crbl*^{rd8} background (DKO *rd8*) exhibits AMD-like focal retinal lesions that include degeneration of photoreceptors and RPE, accumulation of lipofuscin A2E, and immunological features, such as increased deposition of complement factors and macrophages (Chan et al., 2008; Chu et al., 2013; Ramkumar et al., 2010; Ross et al., 2007; Tuo et al., 2007; Zhou et al., 2011), and locate mainly in the inferior posterior pole. Although there has been some recent controversy surrounding the model after discovery of the *rd8* mutation in C57BL/6N mouse (Luhmann et al., 2012; Mattapallil et al., 2012; Vessey et al., 2012), and the rd8 mutation is critical for the development of focal retinal degeneration in DKO *rd8* mice, it is clear that these important AMD-like phenotypes in DKO *rd8* that track the pathology of human patients are in addition to the mild retinal dystrophy associated with the *Crbl*^{rd8} background found in C57BL/6N mouse (Chu et al., 2013; Mattapallil et al., 2012). Moreover, it has been demonstrated that potential AMD therapeutic interventions, such as enriched omega-3 diet and AAV5-mediated sFLT01 gene therapy effectively arrested AMD-like focal retinal lesions on DKO *rd8* mice (Tuo et al., 2009, b). While the exact mechanisms by which these genes and their products interact are unclear, the strain still remains a useful tool for AMD research.

The main reason for central vision loss in human AMD is likely cone degeneration rather than rod death (Mustafi et al., 2009). However, the debate on whether cones or rods are more affected is still ongoing. Photoreceptor topography studies with mid- to late-stage

AMD patients suggest rods are preferentially more vulnerable than cones because parafoveal rods degenerate early whereas foveal cones appear to be well preserved (Curcio et al., 1993, 1996). However, a study on aging and AMD patients demonstrated anomalies in the cone distal axon and extensive redistribution of cone L/M opsin (Shelley et al., 2009), suggesting that cones may be susceptible in AMD. This result is consistent with the finding of fewer or no detectable synaptic ribbons in the photoreceptor terminals over drusen in AMD patients (Johnson et al., 2005). Although functional studies reveal the involvement of cones and rods in AMD (Curcio et al., 1993, 1996; Hogg and Chakravarthy, 2006; Jackson et al., 2002; Owsley et al., 2001), the morphological discrepancies mentioned have yet to be resolved, particularly on the subcellular level for photoreceptor terminals. In addition, the extent of photoreceptor damage and distribution of photoreceptor pigments remain unclear in early AMD. Using multiple morphological techniques, we investigated photoreceptor loss, subcellular changes of photoreceptor synapses, expression of synapse-associated proteins, and photoreceptor opsin and their histopathological susceptibility to damage in DKO *rd8* mice at one month of age.

MATERIALS AND METHODS

Animals

Ccl2$^{-/-}$ mice (obtained from Drs. Bao Lu and Barrett Rollins of Children's Hospital, Harvard Medical School) were crossed with *Cx3cr1*$^{-/-}$ mice (provided by Dr. Philip Murphy of the NIAID/NIH), strains which were recently identified on the C57BL/6N *rd8* background (C57BL/6N, Mattapallil et al., 2012), to generate a double knock out *Ccl2*$^{-/-}$ and *Cx3cr1*$^{-/-}$ mice (DKO *rd8* mice, Chan et al., 2008; Tuo et al, 2007). C57BL/6N and DKO *rd8* mice were bred in a 12-h light/12-h dark cycle house. Care and handling of animals were approved by the Institutional Animal Care and Use Committee in accordance with the NIH guidelines.

Tissue preparation of light microscopy immunofluorescence

Retinal tissue for light microscopy (LM) immunofluorescence study was prepared as described previously (Zhang and Diamond, 2006). Briefly, mice were euthanized by CO2, and then both eyes were removed and hemisected. Six DKO *rd8* and four C57BL/6N mouse eyes at one month of age were used. The cornea, lens, and vitreous were removed under a dissecting microscope. The posterior eyecups were fixed in 4% paraformaldehyde in 0.1 M phosphate buffer (PB) at pH 7.4 for 15 to 30 min at room temperature (RT). For frozen sections, the eyecups were cryoprotected in graded sucrose solutions (10, 20, and 30% w/v, respectively), and cryostat sections were cut at 14 μm, mounted, and stored at −20°C. For retinal whole mounts, three retinas from mice 4 weeks of age were isolated from the eyecups and then cryoprotected, which were processed free floating.

Immunofluorescence

The sources and working dilutions of primary antibodies are listed in Table I. The primary antibodies were diluted in phosphate buffer saline (PBS, pH 7.4) containing 2% NDS, 1% bovine serum albumin (BSA, Sigma), 0.3% Triton X-100. Retinal sections were rinsed, blocked 1 h in 5% donkey serum, and incubated in primary antibodies overnight at 4°C. After washes in PBS, appropriate secondary antibodies conjugated to FITC, Cy3, or Cy5 (1:200–400; Invitrogen) were applied for 2 h at RT. In double- and triple-labeling experiments, sections were incubated in a mixture of primary antibodies followed by a mixture of secondary antibodies. Whole mount retinas were incubated for 5 to 6 days in an antibody-against CtBP2 (1:100) and for 2 days in the secondary antibody. Slides and whole mounts were rinsed before and after antibody incubations and finally cover-slipped with Vecta shield with or without DAPI (Vector). Immunofluorescence was visualized with a

Zeiss LSM-510 confocal microscope through 40×/1.0 and 63×/1.4 oil immersion objectives at a resolution of 1024 × 1024 pixels. For whole mount retinas, stacks of 15 optical sections were scanned with a step of one micron using LSM5 Pascal 3 software, from which 62 randomly selected synaptic ribbons were analyzed in NIH ImageJ to determine their mean lengths. The brightness and the contrast of the final images were adjusted using Adobe Photoshop 6.

Tissue preparation of electron microscopy (EM)

Retinal tissue for EM study was prepared as described previously (Zhang and Diamond, 2006). Briefly, a total of 4 mice at one month of age were used for EM study. Strips (1–2 mm × 2–4 mm) of eye posterior segment (around the optic disc) were fixed in 2% paraformaldehyde and 2% glutaraldehyde in 0.1 M PB, pH 7.4 for 12 h at RT. After washing with rinsing buffer (RB, 4% sucrose and 0.15 mM $CaCl_2$ in PB, pH 7.4 at 4°C), tissues were then postfixed in 1% OsO_4 in 0.1 M PB for 1 h at 4°C. After rinsing and dehydration, tissues were embedded in Durcupan resin for 72 h at 60° C. Regions of interest for EM examination were pre-screened on one micron thick sections stained with toluidine blue under LM. Then 70 to 90 nm ultrasections were collected in 200 mesh grids, counterstained with 5% uranyl acetate and 0.3% lead citrate. Ultrasections were viewed on a JEOL 1010EM at 60 KV and digital images were acquired at ×8000 to ×30,000 magnifications by AMT software (Advanced Microscopy Techniques, Corp.).

EM quantitative analysis

Forty photomontage images, with a total area of 5280 μm^2 in the outer plexiform layer (OPL), were obtained in C57BL/6N and DKO *rd8* groups. In DKO *rd8* mice, only regions of the OPL over the lesions (outward migrating photoreceptor nuclei) were analyzed. Synaptic terminals of cone and rod were identified based on previous morphological studies of rodent retina. Briefly, cone pedicles are large in size and show electron-lucent appearance containing multiple synaptic ribbons, whereas rod spherules are small in size and show electron-dense appearance containing only one synaptic ribbon (Carter-Dawson and La Vail, 1979). The number of photoreceptor terminals and synaptic ribbons was quantified.

Cell counting

A total photoreceptor count was conducted on LM images. One micron sections from the resin blocks were stained with 1% toluidine blue and photoreceptor nuclei in a fixed area were manually counted. The fixed areas included the entire lesion covering the OPL to the RPE plus 50 μm adjacent to the lesion in DKO *rd8* mice and the same area in C57BL/6N mice. Ultrasections containing these fixed areas were cut for EM. Cone and rod were identified, based on their distinct nucleus heterochromatin (Carter-Dawson and LaVail, 1979), and counted on low power EM images.

Data analysis

Statistical analysis was performed using Stata 8 (Stata, College Station, TX). Numerical data are presented as mean ± SD. Two-tailed Student's *t*-tests were used to compare the means. Chi-square test was used to compare the distribution of the photoreceptor terminals. Significance was concluded at $P < 0.05$.

RESULTS

Early focal morphological changes of photoreceptors and RPE in DKO *rd8* mice

Histological and immunohistochemical analysis exhibited displacement of photoreceptors in opposite directions in C57BL/6N and DKO *rd8* mice (Fig. 1). In C57BL/6N mice, most

retinal architecture was intact at low magnification (Figs. 1A and 1C). Occasionally, a few clusters of photoreceptor nuclei, visualized by DAPI staining, protruded toward the inner nuclear layer (INL) as the early dystrophic retinal lesions (Figs. 1A–1D). Concomitantly, synaptophysin-labeled photoreceptor terminals (Fig. 1B), calbindin D-labeled HCs (Fig. 1D), and PKC-labeled rod BCs (RBCs, data not shown) also extended into the INL. Although the number of inward protrusions of photoreceptors was variable in individual region, the outer margin of the outer nuclear layer (ONL) appeared normal. In contrast, some photoreceptor nuclei protruded into the outer retina, resulting in an irregular outer margin of the ONL in DKO *rd8* mice (Figs. 1F, 1G, and 1H). Such lesions were rarely observed in C57BL/6N mice. Furthermore, postsynaptic RBC dendrites (Fig. 1E) and presynaptic photoreceptor ribbons (Figs. 1G and 1H) labeled by PKC-and CtBP2-antibodies, respectively, were located in the ONL, suggesting ectopic synapses in the outer retina (also see Figs. 7 and 8). Similar outward migrating photoreceptor nuclei were also evident in pre-screened thick sections and low power EM images of DKO *rd8* mice, a phenotype which were noticeably absent in C57BL/6N mice (Figs. 2A–2D, 2G1, and 2H1). Importantly, EM data illustrated that, unlike in C57BL/6N mice, there were significantly more aggregated lipofuscin-like lysosomes in the RPE and thickening of Bruch's membrane in DKO *rd8* mice (Figs. 2G2 and 2H2). These findings are in agreement with our previous studies (Ramkumar et al., 2010; Tuo et al., 2007, 2012a). Moreover, LM cell counting indicated a significant reduction of photoreceptors (~17%) over the focal lesion region when compared with areas 50 microns away from the lesions in DKO *rd8* (53 ± 8.6 vs. 69 ± 2.6, $P = 0.000186$) or from C57BL/6N mice (53±8.6 vs. 70±3.9, $P = 0.000149$, respectively) (Fig. 2E). Furthermore, cell counting in EM images established that cone nuclei made up approximately 4% of the photoreceptor nuclei in DKO *rd8* mice when compared with 7% in C57BL/6N mice (Fig. 2F).

Reduced expression and ectopic location of synapse associated proteins in DKO *rd8* mice

To investigate whether photoreceptor terminals were also damaged due to degeneration of the photoreceptor somata, CtBP2 immunostaining was performed in C57BL/6N and DKO *rd8* mice, respectively. In the retinal vertical sections, intensely continuous CtBP2 labeling was evident in the outer plexiform layer (OPL) in C57BL/6N mice (Fig. 3A). In DKO *rd8* mice, however, CtBP2 labeling in the OPL was markedly reduced and scarce CtBP2 punctas were visible in the ONL (Fig. 3B). In whole mount retinas, CtBP2 immunoreactivity show an even distribution of ribbons in the OPL in C57BL/6N mice (Fig. 3C), in contrast to apparent focal loss of ribbons in the OPL in DKO *rd8* mice (Fig. 3D), even after a stack of 15 frames Z-axis scan (1 μm step) were collected to rule out loss of fluorescent signals due to tissue folding (data not shown). The mean intensity of CtBP2 expression in whole mount retinas was significantly greater in C57BL/6N mice than in DKO *rd8* mice (Fig. 3E, $P = 0.001$, $n = 4$ eyes in each). Length of synaptic ribbons was significantly different between DKO *rd8* and C57BL/6N mice (1.1 ± 0.3 μm vs. 1.8 ± 0.3 μm, respectively, $P = 0.0001$) (Fig. 3F, $n = 62$ in each).

We also evaluated the distribution of synaptophysin, a major synaptic vesicle protein, and vesicular glutamate transporter 1 (VGLUT1), a protein participating in glutamate synaptic transmission in the CNS including retina. Similar to CtBP2, both synaptophysin and VGLUT1 labeling was found primarily in the OPL, and occasionally in the INL in C57BL/6N mice (Figs. 4A, 4B, and 4E). In DKO *rd8* mice, however, labeling of both proteins was readily visible in the ONL (Figs. 4C, 4D, and 4F).

Mislocalized or reduced expression of photoreceptor pigments in DKO *rd8* mice

Immunohistochemical study of cone-opsin and rod rhodopsin expression was carried out in retinal sections taken from vertical planes near the optic nerve in C57BL/6N and DKO *rd8*

mice. In C57BL/6N mice, the co-expression of S- and M-opsin was evident in ventral (Figs. 5A1–5A3) and dorsal cone OS (Figs. 5C1–5C3), although a few S-opsin did not show Mopsin labeling (arrow in Fig. 5A3), consistent with reported results in wild type mice (C57/BL6J without *rd8* background) (Applebury et al., 2000; Haverkamp et al., 2005). In DKO *rd8* mice, however, S-opsin labeling was dramatically decreased in both ventral and dorsal regions, resulting in the reduced area of retina with co-expression of S- and M-opsins (Figs. 5B1–5B3, 5D1–5D3). Meanwhile, S-opsins in the ventral region are more extensively mislocalized throughout the inner segment (IS), ONL, OPL, and even INL (Fig. 5B1), whereas those in dorsal region show less mislocalization (Fig. 5D1). M-opsin in both ventral and dorsal region was widely mislocalized in cytoplasmic membranes of soma and axons, particularly in cone pedicles (Figs. 5B2 and 5D2), which were barely labeled for S-opsin. Interestingly, rhodopsin mislocalization appeared less significant relative to cone opsin in DKO *rd8* mice. Rhodopsin labeling in the ventral region was mainly concentrated in the IS and INL but scarcely seen in the soma, axons and OPL in DKO *rd8* mice (Figs. 5C1–5C3). These results suggested that cone opsins were more extensively redistributed and more severely reduced than rhodopsin in DKO *rd8* mice.

Distinct abnormalities of cone and rod terminals in DKO *rd8* mice

To further examine the early subcellular changes of abnormal terminals, EM was conducted on C57BIV 6N and DKO *rd8* mice. In C57BL/6N mice retina, cone pedicles and rod spherules were tightly organized and packed as a regular band in the OPL (Fig. 6A). Both cone and rod terminals contained synaptic ribbons (Figs. 6B and 6C; arrows) characterized by electron-dense rod-shaped profiles that are surrounded by numerous synaptic vesicles, and form deep invaginated ribbon synapses with two HC processes and one RBC dendrite (Fig. 6B). In DKO *rd8* mice retina, however, both types of terminals exhibit several distinct ultrastructural alterations. First, photoreceptor terminals in the OPL were highly disorganized such that a normal band of terminals, as shown in Figure 6A, was disrupted (Fig. 6D). Second, deep synaptic invaginations at axon terminals were shallower or flattened, resulting in seeming extrusion of postsynaptic elements (Figs. 6E and 6F). Third, two terminals appeared to be rare synaptic ribbons (Figs. 6E and 6F), and remaining ribbons were shortened (arrow in Fig. 6E) or floating in the cytoplasm (Fig. 6E, double arrows), which is consistent with LM results. Fourth, some cone pedicles contained numerous vacuoles and swelling mitochondrial, resulting in an extremely lucent and atrophic appearance (Figs. 6E and 6F). In contrast, rod terminals showed a lesser degree of damage, suggesting different degenerative stages between the two types of photoreceptors. Fifth, rod spherules but not cone pedicles retracted into the ONL, consistent with our LM results, where ectopic synaptic contacts were formed with processes of HC and RBC (Fig. 7).

To precisely evaluate these abnormalities, we sampled 1497 and 1427 photoreceptor terminals under EM in C57BL/6N and DKO *rd8* mice, respectively, and counted the distribution of cone and rod, and determined presence of ribbon in terminals (Table II). The results showed that the number of cone pedicles was four times greater in C57BL/6N than DKO *rd8* (8% vs. 2%), suggesting cone terminals were significantly reduced in DKO *rd8* mice ($P < 0.01$). The percentage of non-ribbon cone terminals was three times greater in DKO *rd8* than C57BL/6N mice (41% vs. 17%, $P < 0.01$). A similar ratio was also recorded in rod terminals (58% vs. 32% in DKO *rd8* and C57BL/6N mice, respectively, $P < 0.01$).

Remolding of RBC and HC processes, but not cone bipolar cells, in DKO *rd8* mice

To investigate the responses of cone bipolar cells (CBC), RBC, and HC to the degeneration of photoreceptor terminals, double-immunofluorescent labeling with antibodies against HCN4, CaB5, PKC, calbindin-D, and CtBP2 was performed on retinal sections of C57BL/6N and DKO *rd8* mice. HCN4 was expressed in OFF-CBC, whereas CaB5 was in both ON-

CBC and a few RBC. The OFF-CBC dendrites were exclusively in the OPL in both C57BL/6N and DKO *rd8* mice, even though CtBP2 punctas were visible in the ONL in DKO *rd8* mice (Figs. 8A–8C), suggesting that lack of OFF-CBC sprouting. CaB5 labeled dendrites were exclusively in the OPL in C57BL/6N mice (Fig. 8D) but a few dendrites were evident in the ONL in DKO *rd8* mice (Figs. 8E and 8F). The latter pattern was similar to PKC labeled RBC, which showed a close association between sprouted dendrites and CtBP2-labeled synaptic ribbons (Figs. 8H and 8I). Thus, CaB5 labeled dendrites in the ONL (Fig. 8E) most likely originated from RBC rather than CBC. Similarly, calbindin-D labeled HC processes extended into the ONL and showed an association with ectopic CtBP2 puncta (Figs. 8K and 8L).

Expression of glutamate receptors in the sprouting of RBC and HC processes

To investigate the possible functional involvement of ectopic rod synapses observed by EM, double-labeling experiments of specific glutamate receptor antibodies with markers for RBC and HC were performed on DKO *rd8* mice. An antibody against mGluR6 is an activity-dependent marker for ON-pathway including the dendrites of RBC (Nomura et al., 1994; Vardi and Morigiwa, 1997), whereas an antibody against GluR2/3, ionotropic glutamate receptor, is a marker associated to the processes of HC. The results showed that both mGluR6 (Fig. 9A; A1–A3) and GluR2/3 (Fig. 9B; B1–B2) puncta were ectopically expressed in the sprouting of RBC dendrites and HC processes, respectively, suggesting that the extended dendrites and processes are likely functional.

DISCUSSION

Early degeneration of photoreceptors and RPE in DKO *rd8* mice

This study confirms focal retinal lesions with abnormalities in Bruch's membrane, RPE, and photoreceptor cells, as well as elevated ocular A2E in the DKO *rd8* mice, as evidenced in our previous studies (Chan et al., 2008; Tuo et al., 2007). Although photoreceptor loss has been mentioned in various AMD mouse models (Ramkumar et al., 2010), the proportion of photoreceptors affected in the early stage of disease remains unclear. Our study demonstrates an approximate 17% reduction of photoreceptors within lesion sites in DKO *rd8* mice (Fig. 2E), which is comparable to a previous study citing 30% reduction of photoreceptors over drusen in human AMD eyes (Johnson et al., 2005). The lesions with reduced photoreceptors are focal since no reduction is seen at 50 μm surrounding the lesion. Thus, these early focal retinal lesions in DKO *rd8* mice may not be detectable by electroretinography (ERG) as evidenced in *Crb1*^{rd8} mouse exhibiting large areas of retinal atrophy (Aleman et al., 2011). However, focal-field ERG is required to examine the function of cones, as local cone nuclei were reduced in the ONL (Fig. 2F). It is suggested that photoreceptor degeneration, primarily over the drusen may eventually lead to cell death in AMD patients (Curcio et al., 1993, 1996; Johnson et al., 2005). The reduction of cone photoreceptors at lesion sites suggest an initial, primary lesion-based degeneration as pointed out in a recent study (Zhou et al., 2011).

The reason for photoreceptor atrophy might be attributed to several factors. First, numerous studies cite the phagocytosis of atrophied RPEs (Khandhadia et al., 2012; Klein et al., 1992; Lopez et al., 1996), because photoreceptors and RPE cells maintain an intimate structural and functional relationship (Johnson et al., 2005) and residual bodies as well as lipofuscin accumulation are increased in the RPE (Ramkumar et al., 2010; Tuo et al., 2007; Fig. 1B2). Second, Fas/FasL mediated apoptosis is involved in photoreceptor degeneration (Dunaief et al., 2002; Zacks et al., 2007) and has been reported in DKO *rd8* mice (Cao et al., 2010). A third factor might be related to the activation of microglia and Müller cells, which may cause adjacent photoreceptor death (Ross et al., 2007; Shen et al., 2011; Tuo et al., 2007;

Zhou et al., 2009). In addition, light can also intensify the degenerative process of the photoreceptors (Ambati et al., 2003; Lai et al., 1978).

Cone degeneration is more severe than rod degeneration in young DKO *rd8* mice

A study in the $LRAT^{-/-}$ model suggested that cone opsin plays a major role in determining the degeneration rate of cones (Zhang et al., 2011). Our immunohistochemical data in DKO *rd8* mice shows that S-opsin expression is dramatically reduced, whereas M-opsin is more extensively redistributed when compared with rhodopsin, suggesting that cone opsins may be more prone to damage in DKO *rd8* retina. This is in agreement with a study from aging non-AMD patients (Shelley et al., 2009). To our knowledge, this is the first morphological evidence showing distinct reduction and/or mislocalization of photoreceptor opsins in an AMD animal model. Similar reduction or redistribution of cone opsin was well-documented to precede cell death in other retinal degeneration models that manifests early cone degeneration (Fisher et al., 2001; Jacobson et al., 2007; Vasireddy et al., 2006; Zhang et al., 2011; Znoiko et al., 2005).

Approximately 50% of cone and rod terminals lose their synaptic ribbons and surviving ribbons are shortened and/or floating in the cytoplasm, suggesting that both cones and rods are degenerative at this stage. This finding is similar with what has been illustrated in AMD patients that show fewer or no detectable synaptic ribbons over drusen (Johnson et al., 2005). Preferential reduction if cone terminals and atrophy in the surviving cone terminals both suggest that cone damages occur earlier than are rods. This result supports the notion that cones are more susceptible to damage in human AMD (Shelley et al., 2009). As a result, the glutamate transmission from affected photoreceptors to postsynaptic targets is likely diminished due to these synaptic abnormalities. Although further functional investigations including multifocal ERG or postsynaptic recording are warranted to confirm this notion, a recent functional study has demonstrated that acute disruption of synaptic ribbons, even without affecting the ultrastructure of the ribbon, markedly reduces both sustained and transient components of neurotransmitter release in mouse bipolar cells and salamander cones (Snellman et al., 2011).

Plasticity of rod but not cone synapse in DKO *rd8* mice

Although ectopic photoreceptor synapses have been described during the late stage in mouse models of various retinal degeneration and detachment (Chang et al., 2008; Gouras and Tanabe, 2003; Lewis et al., 1998; Marc et al., 2003; Peng et al., 2000), little is known about similar changes in AMD mouse models. A close association of CtBP2 with PKC and Calbindin indicates a structural relationship between ectopic synaptic ribbons and the sprouting of RBC and HC. EM analysis further confirms normally structured ectopic rod ribbon synapses in the ONL, compatible with a report in AMD patients (Sullivan et al., 2007) and results in other retinal degeneration models (Lewis et al., 1998; Marc et al., 2003; Peng et al., 2000). Our results imply that photoreceptor terminals have a structural plasticity in response to retinal disorders (Li et al., 1995; Specht et al., 2007; Zhang et al., 2005). Moreover, the co-localization of mGluR6, an activity-dependent marker for ON-pathway (Nomura et al., 1994; Vardi and Morigiwa, 1997) with ectopic RBC dendrites and the co-localization of GluR2/3 with ectopic HC processes strongly suggest that ectopic rod synapses are most likely functional, though immunogold EM and functional investigations are still required to confirm this hypothesis. This reminiscent of aged remodeling of aberrant processes of ON-bipolar cell (Liets et al., 2006; Terzibasi et al., 2009). In contrast, there is no sprouting of CBC and no ectopic cone synapses in the ONL in DKO *rd8* mice, consistent with an observation made from AMD patient samples (Gouras and Tanabe, 2003) and results in other retinal degeneration mouse models (Lee et al., 2012; Lewis et al., 1998; Marc et al., 2003; Phillips et al., 2010). The discrepancy in plasticity between cones and

rods remains unclear; however, that ectopic contacts develop at the tips of RBC dendrites in retinal development, suggests the rod pathway might possess a more robust capacity to form ectopic synapse (Bayley and Morgans, 2007; Liets et al., 2006). This may also imply that cones are more inclined to lesions than rods, or another possibility is that RBC dendrites were mechanically retracted by rod spherules (Fisher et al., 2005). It would be of interest to address this issue with further functional studies.

Are synaptic abnormalities observed here due to *Crb1*^{rds} alone?

Although it can be argued that synaptic abnormalities presented here in DKO *rd8* mice are solely due to *rd8* mutation with retinal dystrophy (Aleman et al., 2011; Chang et al., 2002; Luhmann et al., 2012; Mattapallil et al., 2012; Mehalow et al., 2003; Vessey et al., 2012), several distinct histopathology and immunology differences between C57BL/6N and DKO *rd8* mice are recognized by Chu et al. (2013) and the present results.

Distinct inward vs. outward migrating photoreceptor nuclei were found in C57BL/6N and DKO *rd8* mice (Figs. 1 and 2), respectively, suggesting different **spatial** patterns of photoreceptor degeneration in these two strains. Moreover, outward migrating photoreceptor nuclei were prominent in DKO *rd8* mice at one month whilst inward retinal folds or rosettes that are typical lesions for Crbl^{rd8} mice usually appear at 5 weeks (Chang et al., 2002), indicating that there may exist different **temporal** patterns of photoreceptor degeneration in these two lines. These different photoreceptor degeneration patterns exclude the possibility that synaptic changes observed here are due to *rd8* background alone.

Furthermore, liposuscin A2E level in DKO *rd8* mice was found to be at least three times higher than that in C57BL/6N, *Crb1*^{rd8}, or C57BL/6J mice, consistent with the ultrastructural evidence of lipofuscin accumulation in RPE of DKO *rd8* mice (Chu et al., 2013). Additionally, more active immunological markers were detected in DKO *rd8* compared with other three strains (Chu et al., 2013). These distinct immunopathological features render DKO *rd8* mice a suitable model of AMD, even though the exact mechanism of pathogenesis in DKO *rd8* mice might be complicated by possible interactions of *Ccl2, Cx3cr1*, and other genes in C57BL/6N. It can be used for screening potential AMD drugs and therapies (Chu et al., 2013; Patel et al., 2008). For example, the AMD-like lesions, but not the minor retinal dystrophy found in C57BL/6N, were alleviated with TSG-6 recombinant protein, AAV5-mediated sFLT01 gene therapy, naloxone, or quercetin (Shen et al., 2011:see Fig. 2; Tuo et al., 2012a: see Fig. 2; 2012b: see Fig. 3; also see Cao et al., 2010: Fig. 5). These results further suggest that degeneration in C57BL/6N-related *rd8* background, which manifests as retinal dystrophy toward the inner retina, is different from that in *Ccl2*$^{-/-}$/*Cx3cr1*$^{-/-}$ modification of the *rd8* mutation, which shows focal retinal AMD-like lesions. Further molecular and functional investigations are required to explore the underlying mechanisms.

CONCLUSIONS

This study demonstrates, for the first time, that cone synapse and opsin, but not rod synapse and rhodopsin, are markedly decreased in focal retinal degenerative lesions in the early phase of photoreceptor degeneration in DKO *rd8* mice, and that some rod spheres, but not cone pedicles, form ectopic synapses with postsynaptic processes that express glutamate receptors. Such distinct changes may imply that cones are likely more vulnerable to damage in DKO *rd8* mutation.

Acknowledgments

The authors thank Xi K. Chu for English editing.

Contract grant sponsor: Intramural Research Program of National Eye Institute, NIH.

REFERENCES

Aleman TS, Cideciyan AV, Aguirre GK, Huang WC, Mullins CL, Roman AJ, Sumaroka A, Olivares MB, Tsai FF, Schwartz SB, Vandenberghe LH, Limberis MP, Stone EM, Bell P, Wilson JM, Jacobson SG. Human CRB1-associated retinal degeneration: Comparison with the *rd8* Crb1-mutant mouse model. Invest Ophthalmol Vis Sci. 2011; 52:6898–6910. [PubMed: 21757580]

Ambati J, Anand A, Fernandez S, Sakurai E, Lynn BC, Kuziel WA, Rollins BJ, Ambati BK. An animal model of age-related macular degeneration in senescent *Ccl2*$^{[minus]2[minus]}$ or *Ccr*$^{[minus]2[minus]}$ deficient mice. Nat Med. 2003; 9:1390–1397. [PubMed: 14566334]

Anastasopoulos E, Kakoulidou A, Coleman AL, Sinsheimer JS, Wilson MR, Yu F, Salonikiou A, Koskosas A, Pappas T, Founti P, Lambropoulos A, Topouzis F. Association of sequence variation in the CX3CR1 gene with geographic atrophy age-related macular degeneration in a Greek population. Curr Eye Res. 2012; 37:1148–1155. [PubMed: 22816662]

Applebury ML, Antoch MP, Baxter LC, Chun LL, Falk JD, Farhangfar F, Kage K, Krzystolik MG, Lyass LA, Robbins JT. The murine cone photoreceptor: A single cone type expresses both S and M opsins with retinal spatial patterning. Neuron. 2000; 27:513–523. [PubMed: 11055434]

Bayley PR, Morgans CW. Rod bipolar cells and horizontal cells form displaced synaptic contacts with rods in the outer nuclear layer of the nob2 retina. J Comp Neurol. 2007; 500:286–298. [PubMed: 17111373]

Cao X, Liu M, Tuo J, Shen D, Chan CC. The effects of quercetin in cultured human RPE cells under oxidative stress and in *Ccl2/Cx3cr1* double deficient mice. Exp Eye Res. 2010; 91:15–25. [PubMed: 20361964]

Carter-Dawson LD, LaVail MM. Rods and cones in the mouse retina. I. Structural analysis using light and electron microscopy J Comp Neurol. 1979; 188:245–262.

Chan CC, Ross RJ, Shen D, Ding X, Majumdar Z, Bojanowski CM, Zhou M, Salem N Jr, Bonner R, Tuo J. *CcZ2*/Cx3crl-defi-cient mice: An animal model for age-related macular degeneration. Ophthalmic Res. 2008; 40:124–128. [PubMed: 18421225]

Chan CC, Tuo J, Bojanowski CM, Csaky KG, Green WR. Detection of *CX3CR1* single nucleotide polymorphism and expression on archived eyes with age-related macular degeneration. Histol Histopathol. 2005; 20:857–863. [PubMed: 15944936]

Chang B, Hawes NL, Hurd RE, Davisson MT, Nusinowitz S, Heck-enlively JR. Retinal degeneration mutants in the mouse. Vision Res. 2002; 42:517–525. [PubMed: 11853768]

Chang B, Dacey MS, Hawes NL, Hitchcock PF, Milam AH, Atmaca-Sonmez P, Nusinowitz S, Heckenlively JR. Cone photoreceptor function loss-3, a novel mouse model of achromatopsia due to a mutation in Gnat2. Invest Ophthalmol Vis Sci. 2006; 47:5017–5021. [PubMed: 17065522]

Chang B, Mandal MN, Chavali VR, Hawes NL, Khan NW, Hurd RE, Smith RS, Davisson ML, Kopplin L, Klein BE, Klein R, Iyengar SK, Heckenlively JR, Ayyagari R. Age-related retinal degeneration (arrd2) in a novel mouse model due to a nonsense mutation in the Mdm1 gene. Hum Mol Genet. 2008; 17:3929–3941. [PubMed: 18805803]

Chu XK, Wang Y, Ardeljan D, Tuo J, Chan CC. Controversial view of a genetically altered mouse model of focal retinal degeneration. Bioengineered. 2013; 4:1–6.

Combadiere C, Feumi C, Raoul W, Keller N, Rodero M, Pezard A, Lavalette S, Houssier M, Jonet L, Picard E, Debre P, Sirinyan M, Deterre P, Ferroukhi T, Cohen SY, Chauvaud D, Jeanny JC, Chemtob S, Behar-Cohen F, Sennlaub F. CX3CR1-depend-ent subretinal microglia cell accumulation is associated with cardinal features of age-related macular degeneration. J Clin Invest. 2007; 117:2920–2928. [PubMed: 17909628]

Curcio CA, Medeiros NE, Millican CL. Photoreceptor loss in age-related macular degeneration. Invest Ophthalmol Vis Sci. 1996; 37:1236–1249. [PubMed: 8641827]

Curcio CA, Millican CL, Allen KA, Kalina RE. Aging of the human photoreceptor mosaic: Evidence for selective vulnerability of rods in central retina. Invest Ophthalmol Vis Sci. 1993; 34:3278–3296. [PubMed: 8225863]

Dick O, tom Dieck S, Altrock WD, Ammermüller J, Weiler R, Garner CC, Gundelfinger ED, Brandstätter JH. The presynaptic active zone protein bassoon is essential for photoreceptor ribbon synapse formation in the retina. Neuron. 2003; 37:775–786. [PubMed: 12628168]

Dowling JE, Boycott BB. Organization of the primate retina: Electron microscopy. Proc R Soc Lond B Biol Sci. 1966; 166:80–111. [PubMed: 4382694]

Dunaief JL, Dentchev T, Ying GS, Milam AH. The role of apoptosis in age-related macular degeneration. Arch Ophthalmol. 2002; 120:1435–1442. [PubMed: 12427055]

Feigl B, Cao D, Morris CP, Zele AJ. Persons with age-related maculopathy risk genotypes and clinically normal eyes have reduced mesopic vision. Invest Ophthalmol Vis Sci. 2011; 52:1145–1150. [PubMed: 20881291]

Fisher SK, Stone J, Rex TS, Linberg KA, Lewis GP. Experimental retinal detachment: A paradigm for understanding the effects of induced photoreceptor degeneration. Prog Brain Res. 2001; 131:679–698. [PubMed: 11420980]

Fisher SK, Lewis GP, Linberg KA, Verardo MR. Cellular remodeling in mammalian retina: Results from studies of experimental retinal detachment. Prog Retin Eye Res. 2005; 24:395–431. [PubMed: 15708835]

Forrester JV. Macrophages eyed in macular degeneration. Nat Med. 2003; 9:1350–1351. [PubMed: 14595424]

Gehrs KM, Anderson DH, Johnson LV, Hageman GS. Age-related macular degeneration--Emerging pathogenetic and therapeutic concepts. Ann Med. 2006; 38:450–471. [PubMed: 17101537]

Gouras P, Tanabe T. Ultrastructure of adult rd mouse retina. Graefes Arch Clin Exp Ophthalmol. 2003; 241:410–417. [PubMed: 12715183]

Haverkamp S, Wässle H, Duebel J, Kuner T, Augustine GJ, Feng G, Euler T. The primordial, blue-cone color system of the mouse retina. J Neurosci. 2005; 25:5438–5445. [PubMed: 15930394]

Hogg RE, Chakravarthy U. Visual function and dysfunction in early and late age-related maculopathy. Prog Retin Eye Res. 2006; 25:249–278. [PubMed: 16580242]

Imai T, Hieshima K, Haskell C, Baba M, Nagira M, Nishimura M, Kakizaki M, Takagi S, Nomiyama H, Schall TJ, Yoshie O. Identification and molecular characterization of fractalkine receptor CX3CR1, which mediates both leukocyte migration and adhesion. Cell. 1997; 91:521–530. [PubMed: 9390561]

Jackson GR, Owsley C, Curcio CA. Photoreceptor degeneration and dysfunction in aging and age-related maculopathy. Ageing Res Rev. 2002; 1:381–396. [PubMed: 12067593]

Jacobson SG, Aleman TS, Cideciyan AV, Heon E, Golczak M, Beltran WA, Sumaroka A, Schwartz SB, Roman AJ, Windsor EA, Wilson JM, Aguirre GD, Stone EM, Palczewski K. Human cone photoreceptor dependence on RPE65 isomerase. Proc Natl Acad Sci USA. 2007; 104:15123–15128. [PubMed: 17848510]

Johnson PT, Brown MN, Pulliam BC, Anderson DH, Johnson LV. Synaptic pathology, altered gene expression, and degeneration in photoreceptors impacted by drusen. Invest Ophthalmol Vis Sci. 2005; 46:4788–4795. [PubMed: 16303980]

Khandhadia S, Cipriani V, Yates JR, Lotery AJ. Age-related macular degeneration and the complement system. Immunobiology. 2012; 217:127–146. [PubMed: 21868123]

Klein R, Klein BE, Linton KL. Prevalence of age-related maculopathy. The Beaver Dam Eye Study. Ophthalmology. 1992; 99:933–943. [PubMed: 1630784]

Lai YL, Jacoby RO, Jonas AM. Age-related and light-associated retinal changes in Fischer rats. Invest Ophthalmol Vis Sci. 1978; 17:634–638. [PubMed: 669893]

Lee DC, Vazquez-Chona FR, Ferrell WD, Tarn BM, Jones BW, Marc RE, Moritz OL. Dysmorphic photoreceptors in a P23H mutant rhodopsin model of retinitis pigmentosa are metabolically active and capable of regenerating to reverse retinal degeneration. J Neurosci. 2012; 32:2121–2128. [PubMed: 22323724]

Lewis GP, Linberg KA, Fisher SK. Neurite out gro*rd*8h from bipolar and horizontal cells after experimental retinal detachment. Invest Ophthalmol Vis Sci. 1998; 39:424–434. [PubMed: 9478003]

Li ZY, Kljavin IJ, Milam AH. Rod photoreceptor neurite sprouting in retinitis pigmentosa. J Neurosci. 1995; 15:5429–5438. [PubMed: 7643192]

Liets LC, Eliasieh K, van der List DA, Chalupa LM. Dendrites of rod bipolar cells sprout in normal aging retina. Proc Natl Acad Sci USA. 2006; 103:12156–12160. [PubMed: 16880381]

Lopez PF, Sippy BD, Lambert HM, Thach AB, Hinton DR. Transdifferentiated retinal pigment epithelial cells are immunoreactive for vascular endothelial gro*rd8h* factor in surgically excised age-related macular degeneration-related choroidal neovascular membranes. Invest Ophthalmol Vis Sci. 1996; 37:855–868. [PubMed: 8603870]

Marc RE, Jones BW, Watt CB, Strettoi E. Neural remodeling in retinal degeneration. Prog Retin Eye Res. 2003; 22:607–655. [PubMed: 12892644]

Mattapallil MJ, Wawrousek EF, Chan CC, Zhao H, Roychoudhury JR, Ferguson TA, Caspi RR. The *rd8* mutation of the *Crb1* gene is present in vendor lines of C57BL/6N mice and embryonic stem cells, and confounds ocular induced mutant phenotypes. Invest Ophthalmol Vis Sci. 2012; 53:2921–2927. [PubMed: 22447858]

Matthews G, Fuchs P. The diverse roles of ribbon synapses in sensory neurotransmission. Nat Rev Neurosci. 2010; 11:812–822. [PubMed: 21045860]

Mehalow AK, Kameya S, Smith RS, Hawes NL, Denegre JM, Young JA, Bechtold L, Haider NB, Tepass U, Heckenlively JR, Chang B, Naggert JK, Nishina PM. CRB1 is essential for external limiting membrane integrity and photoreceptor morphogenesis in the mammalian retina. Hum Mol Genet. 2003; 12:2179–2189. [PubMed: 12915475]

Mustafi D, Engel AH, Palczewski K. Structure of cone photoreceptors. Prog Retin Eye Res. 2009; 28:289–302. [PubMed: 19501669]

Niess JH, Brand S, Gu X, Landsman L, Jung S, McCormick BA, Vyas JM, Boes M, Ploegh HL, Fox JG, Littman DR, Reinecker HC. CX3CR1-mediated dendritic cell access to the intestinal lumen and bacterial clearance. Science. 2005; 307:254–258. [PubMed: 15653504]

Nomura A, Shigemoto R, Nakamura Y, Okamoto N, Mizuno N, Nakanishi S. Developmentally regulated postsynaptic localization of a metabotropic glutamate receptor in rat rod bipolar cells. Cell. 1994; 77:361–369. [PubMed: 8181056]

Owsley C, Jackson GR, White M, Feist R, Edwards D. Delays in rod-mediated dark adaptation in early age-related maculopathy. Ophthalmology. 2001; 108:1196–1202. [PubMed: 11425675]

Patel M, Chan CC. Immunopathological aspects of age-related macular degeneration. Semin Immunopathol. 2008; 30:97–110. [PubMed: 18299834]

Peng YW, Hao Y, Petters RM, Wong F. Ectopic synaptogenesis in the mammalian retina caused by rod photoreceptor-specific mutations. Nat Neurosci. 2000; 3:1121–1127. [PubMed: 11036269]

Phillips MJ, Otteson DC, Sherry DM. Progression of neuronal and synaptic remodeling in the rd10 mouse model of retinitis pigmentosa. J Comp Neurol. 2010; 518:2071–2089. [PubMed: 20394059]

Ramkumar HL, Zhang J, Chan CC. Retinal ultrastructure of murine models of dry age-related macular degeneration (AMD). Prog Retin Eye Res. 2010; 29:169–190. [PubMed: 20206286]

Regus-Leidig H, tom Dieck S, Brandstätter JH. Absence of functional active zone protein Bassoon affects assembly and transport of ribbon precursors during early steps of photoreceptor synaptogenesis. Eur J Cell Biol. 2010; 89:468–475. [PubMed: 20188438]

Ross RJ, Zhou M, Shen D, Fariss RN, Ding X, Bojanowski CM, Tuo J, Chan CC. Immunological protein expression profile in *Ccl2/Cx3cr1* deficient mice with lesions similar to age-related macular degeneration. Exp Eye Res. 2008; 86:675–683. [PubMed: 18308304]

Raoul W, Combadiere C, Keller N, Rodero M, Jeanny JC, Behar-Cohen F, Sennlaub F. Retinal degeneration occurs in *CX3CR1* knockout animals secondary to subretinal microglia accumulation. Invest Ophthalmol Vis Sci. 2007; 48:3023–3027.

Rutar M, Natoli R, Valter K, Provis JM. Early focal expression of the chemokine Ccl2 by Müller cells during exposure to damage-inducing bright continuous light. Invest Ophthalmol Vis Sci. 2011; 52:2379–2388. [PubMed: 21228381]

Savarin-Vuaillat C, Ransohoff RM. Chemokines and chemokine receptors in neurological disease: Raise, retain, or reduce? Neurotherapeutics. 2007; 4:590–601. [PubMed: 17920540]

Shelley EJ, Madigan MC, Natoli R, Penfold #PL, Provis JM. Cone degeneration in aging and age-related macular degeneration. Arch Ophthalmol. 2009; 127:483–492. [PubMed: 19365029]

Shen D, Cao X, Zhao L, Tuo J, Wong RD, Chan CC. Naloxone ameliorates retinal lesions in *Ccl2/Cx3cr1* double-deficient mice via modulation of microglia. Invest Ophthalmol Vis Sci. 2011; 52:2897–2904. [PubMed: 21245403]

Snellman J, Mehta B, Babai N, Bartoletti TM, Akmentin W, Francis A, Matthews G, Thoreson W, Zenisek D. Acute destruction of the synaptic ribbon reveals a role for the ribbon in vesicle priming. Nat Neurosci. 2011; 14:1135–1141. [PubMed: 21785435]

Specht D, tom Dieck S, Ammermüller J, Regus-Leidig H, Gundel-finger ED, Brandstätter JH. Structural and functional remodeling in the retina of a mouse with a photoreceptor synapt-opathy: Plasticity in the rod and degeneration in the cone system. Eur J Neurosci. 2007; 26:2506–2515. [PubMed: 17970721]

Sterling P, Matthews G. Structure and function of ribbon synapses. Trends Neurosci. 2005; 1:20–29. [PubMed: 15626493]

Sullivan RK, Woldemussie E, Pow DV. Dendritic and synaptic plasticity of neurons in the human age-related macular degeneration retina. Invest Ophthalmol Vis Sci. 2007; 48:2782–2791. [PubMed: 17525213]

Sunnemark D, Eltayeb S, Wallström E, Appelsved L, Malmberg A, Lassmann H, Ericsson-dahlstrand A, Piehl F, Olsson T. Differential expression of the chemokine receptors CX3CR1 and CCR1 by microglia and macrophages in myelin-oligodendrocyte-glycoprotein-induced experimental autoimmune encephalomyelitis. Brain Pathol. 2003; 13:617–629. [PubMed: 14655765]

Terzibasi E, Calamusa M, Novelli E, Domenici L, Strettoi E, Cellerino A. Age-dependent remodelling of retinal circuitry. Neurobiol Aging. 2009; 30:819–828. [PubMed: 17920161]

tom Dieck S, Altrock WD, Kessels MM, Qualmann B, Regus H, Brauner D, Fejtov a A, Bracko O, Gundelfinger ED, Brandstätter JH. Molecular dissection of the photoreceptor ribbon synapse: Physical interaction of Bassoon and RIBEYE is essential for the assembly of the ribbon complex. J Cell Biol. 2005; 168:825–836. [PubMed: 15728193]

Tuo J, Smith BC, Bojanowski CM, Meleth AD, Gery I, Csaky KG, Chew EY, Chan CC. The involvement of sequence variation and expression of *CX3CR1* in the pathogenesis of age-related macular degeneration. FASEB J. 2004; 18:1297–1299. [PubMed: 15208270]

Tuo J, Bojanowski CM, Zhou M, Shen D, Ross RJ, Rosenberg KI, Cameron DJ, Yin C, Kowalak JA, Zhuang Z, Zhang K, Chan CC. Murine *Ccl2/Cx3cr1* deficiency results in retinal lesions mimicking human age-related macular degeneration. Invest Ophthalmol Vis Sci. 2007; 48:3827–3836. [PubMed: 17652758]

Tuo J, Ross RJ, Herzlich AA, Shen D, Ding X, Zhou M, Coon SL, Hussein N, Salem N Jr, Chan CC. A high omega-3 fatty acid diet reduces retinal lesions in a murine model of macular degeneration. Am J Pathol. 2009; 175:799–807. [PubMed: 19608872]

Tuo J, Cao X, Shen D, Wang Y, Zhang J, Oh JY, Prockop DJ, Chan CC. Anti-inflammatory recombinant TSG-6 stabilizes the progression of focal retinal degeneration in a murine model. J Neuroinflammation. 2012a; 9:59. [PubMed: 22452753]

Tuo J, Pang JJ, Cao X, Shen D, Zhang J, Scaria A, Wadsworth SC, Pechan P, Boye SL, Hauswirth WW, Chan CC. AAV5-medi-ated sFLTOl gene therapy arrests retinal lesions in *Ccl2*$^{[minus]/[minus]}$/*Cx3cr1*$^{[minus]/[minus]}$ mice. Neurobiol Aging. 2012b; 33:433. e1-433.e10. [PubMed: 21397984]

Vardi N, Morigiwa K. ON cone bipolar cells in rat express the metabotropic receptor mGluR6. Vis Neurosci. 1997; 14:789–794. [PubMed: 9279006]

Vasireddy V, Jablonski MM, Mandal MN, Raz-Prag D, Wang XF, Nizol L, Iannaccone A, Musch DC, Bush RA, Salem N Jr, Sieving PA, Ayyagari R. Elovl4 5-bp-deletion knock-in mice develop progressive photoreceptor degeneration. Invest Ophthalmol Vis Sci. 2006; 47:4558–4568. [PubMed: 17003453]

Vessey KA, Greferath U, Jobling AI, Phipps JA, Ho T, Waugh M, Fletcher EL. *Ccl2/Cx3cr1* knock-out mice have inner retinal dysfunction but are not an accelerated model of age related macular degeneration. Invest Ophthalmol Vis Sci. 2012; 53:7833–7846. [PubMed: 23074204]

Wan L, Almers W, Chen W. Two ribeye genes in teleosts: The role of Ribeye in ribbon formation and bipolar cell development. J Neurosci. 2005; 25:941–949. [PubMed: 15673675]

Xu H, Chen M, Forrester JV. Para-inflammation in the aging retina. Prog Retin Eye Res. 2009; 28:348–368. [PubMed: 19560552]

Yang X, Hu J, Zhang J, Guan H. Polymorphisms in CFH, HTRA1 and CX3CR1 confer risk to exudative age-related macular degeneration in Han Chinese. Br J Ophthalmol. 2010; 94:1211–1214. [PubMed: 20538655]

Zacks DN, Boehlke C, Richards AL, Zheng QD. Role of the Fas-signaling pathway in photoreceptor neuroprotection. Arch Ophthalmol. 2007; 125:1389–1395. [PubMed: 17923548]

Zhang J, Diamond JS. Distinct perisynaptic and synaptic localization of NMDA and AMPA receptors on ganglion cells in rat retina. J Comp Neurol. 2006; 498:810–820. [PubMed: 16927255]

Zhang N, Beuve A, Townes-Anderson E. The nitric oxide-cGMP signaling pathway differentially regulates presynaptic structural plasticity in cone and rod cells. J Neurosci. 2005; 25:2761–2770. [PubMed: 15758186]

Zhang T, Zhang N, Baehr W, Fu Y. Cone opsin determines the time course of cone photoreceptor degeneration in Leber congenital amaurosis. Proc Natl Acad Sci USA. 2011; 108:8879–8884. [PubMed: 21555576]

Zhou Y, Sheets KG, Knott EJ, Regan CE, Tuo J, Chan CC, Gordon WC, Bazan NG. Cellular and 3D optical coherence tomography assessment during the initiation and progression of retinal degeneration in the *Ccl2/Cx3cr1*-deficient mouse. Exp Eye Res. 2011; 93:636–648. [PubMed: 21854772]

Znoiko SL, Rohrer B, Lu K, Lohr HR, Crouch RK, Ma JX. Downregulation of cone-specific gene expression and degeneration of cone photoreceptors in the Rpe65−/− mouse at early ages. Invest Ophthalmol Vis Sci. 2005; 46:1473–1479. [PubMed: 15790918]

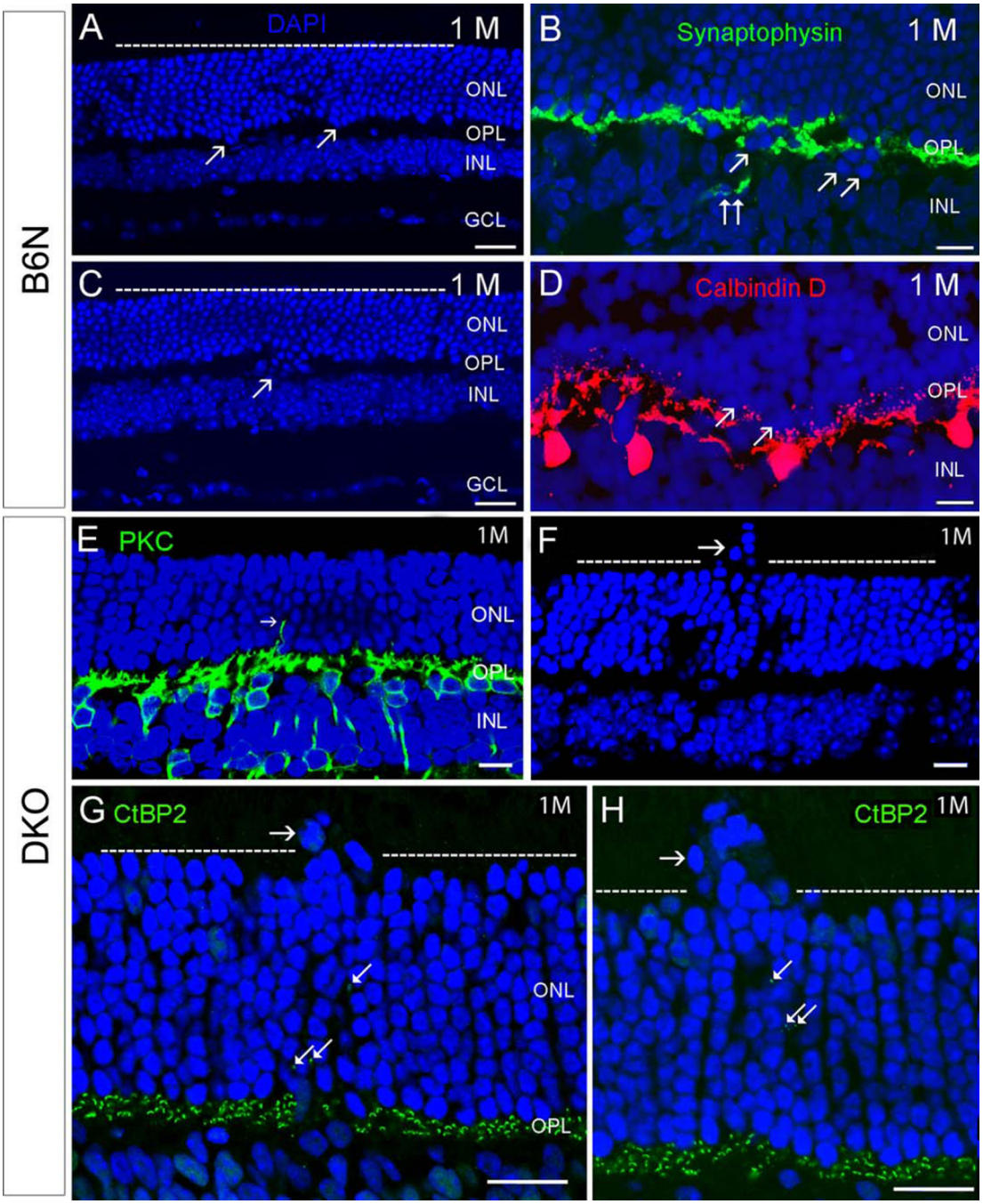

Fig. 1.

Comparison of retinal degeneration between C57BL/6N and DKO *rd8* mice (abbreviates them as B6N and DKO, respectively, in all figures and legends) at one month old. **A–D**: In B6N mice, most of the retinal architecture is unremarkable (A, C). Occasionally, a few or subpopulation of photoreceptor nuclei visualized by DAPI staining, protruded toward the INL in focal regions of retina (arrows in A, C). Correspondingly, a few synaptophysin-labeled photoreceptor terminals (B, double arrows) and Calbindin D-labeled HC (D) extend into the INL. **E–H**: In DKO mice, some photoreceptor nuclei migrate into the retinal inner and outer segments in local regions (horizontal arrows in F, G, and H), resulting in an

irregular outer margin of the ONL (dashed lines in F, G, H). Correspondingly, PKC-labeled RBC dendrites (E, arrow) and CtBP2-labeled synaptic ribbons (arrows in G and H) stretch into the INL. Scale bar: 20 μm for A, C, 10 μm for B, D, E–H. ONL, outer nuclear layer. OPL, outer plexiform layer. INL, inner nuclear layer. IPL, inner plexiform layer. HC, horizontal cell. GCL, ganglion cell layer).

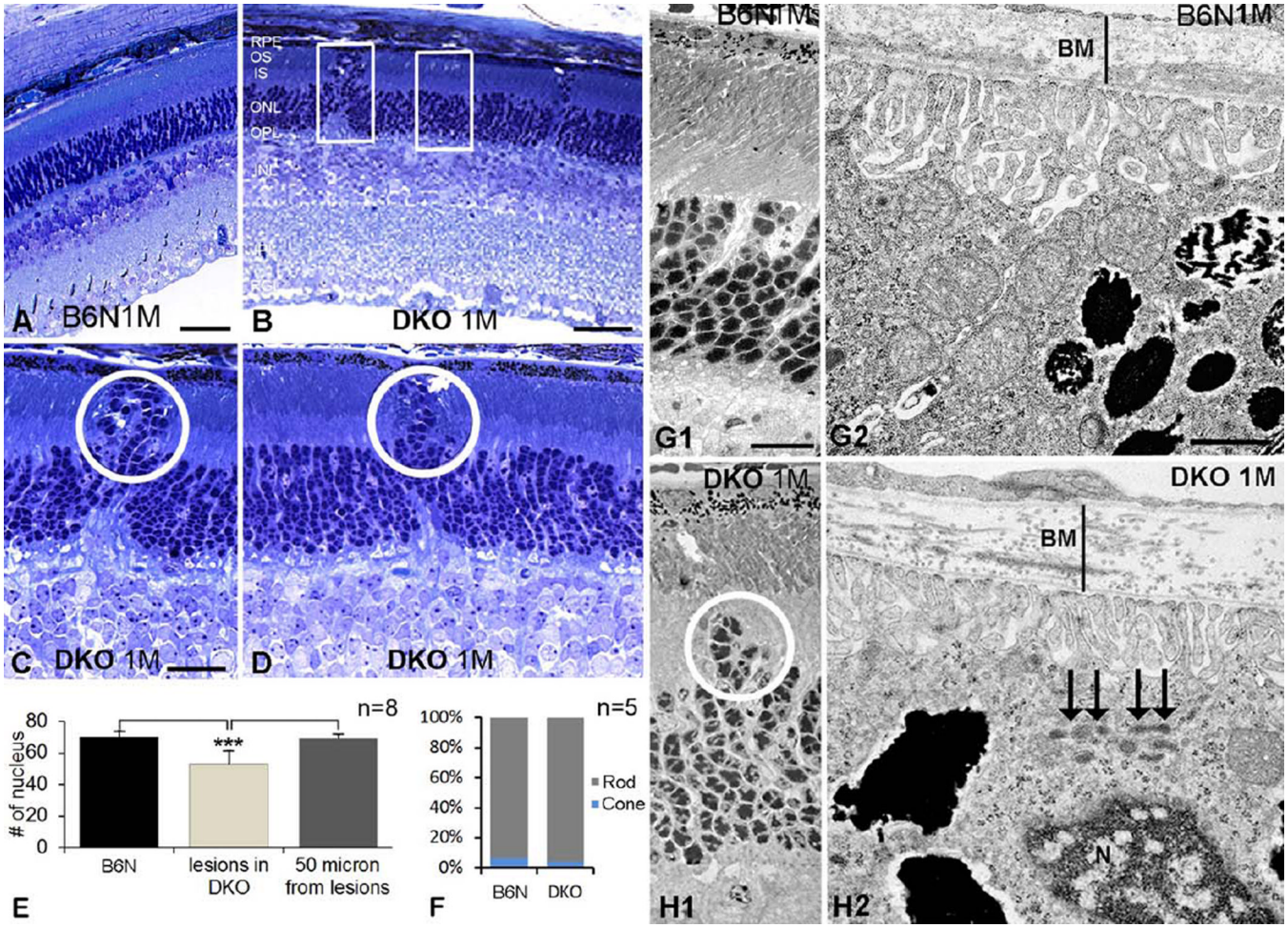

Fig. 2.

Early focal degeneration of photoreceptors and RPE in DKO mice. **A–D**: Histological sections in B6N (A) and DKO (B–D) retinas illustrate outward migrating photoreceptors in low (B) and high magnifications (circles in C, D), which was absent in B6N mice (A). **E**: Histogram shows the number of photoreceptor nuclei in a fixed area (rectangles in B) on B6N and DKO (lesion and 50 μm lateral to the lesion) mice (mean ± SD, $^{**}P < 0.001$). **F**: The percentages of cone and rod nuclei in the ONL in B6N and DKO mice, respectively. **G, H**: EM images show outward migration of photoreceptor nuclei (H1), thickening of Bruch's membrane (H2, a vertical line) and lipofuscin accumulation in the RPE (H2, arrows) in DKO mice, which are not detected in B6N mice (G1–2). Scale bar: 50 μm for A and B, 20 μm for C and D, 500 nm for G1 and H1, 100 nm for G2 and H2.

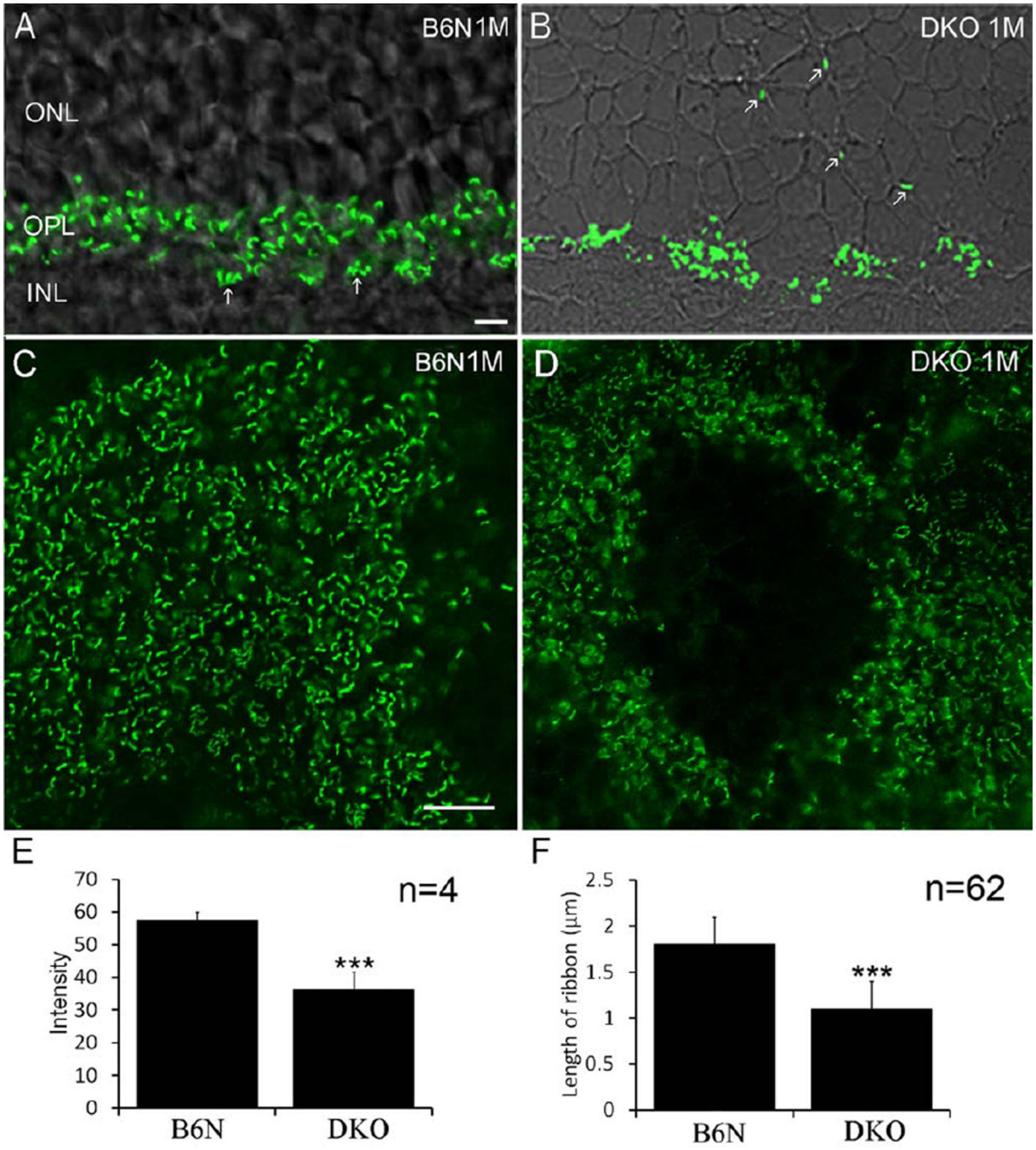

Fig. 3.

Confocal images showing CtBP2 IR immunoreactivity in B6N and DKO mice. **A, B**: On the vertical sections, intense CtBP2 IR is evident in the OPL, in which a cluster of cone pedicles (arrows) is visible in B6N mice (A), whereas CtBP2 labeled puncta are often found in the ONL in DKO mice (B, arrows). **C, D**: In whole mount retinas, CtBP2 labeled synaptic ribbons are rod-like and evenly distribute through the OPL in the B6N mice (C), whereas in the DKO mice there are circular areas lacking CtBP2 IR immunoreactivity and surviving synaptic ribbons are ring-shaped (D). **E**: The mean intensity of CtBP2 IR in DKO mice is two times less than that in B6N mice (mean ± SD, ***$P < 0.001$). **F**: The mean length of

ribbon is significantly shorter in DKO groups (mean ± SD, ***$P < 0.001$). Scale bar: 10 μm for A–D.

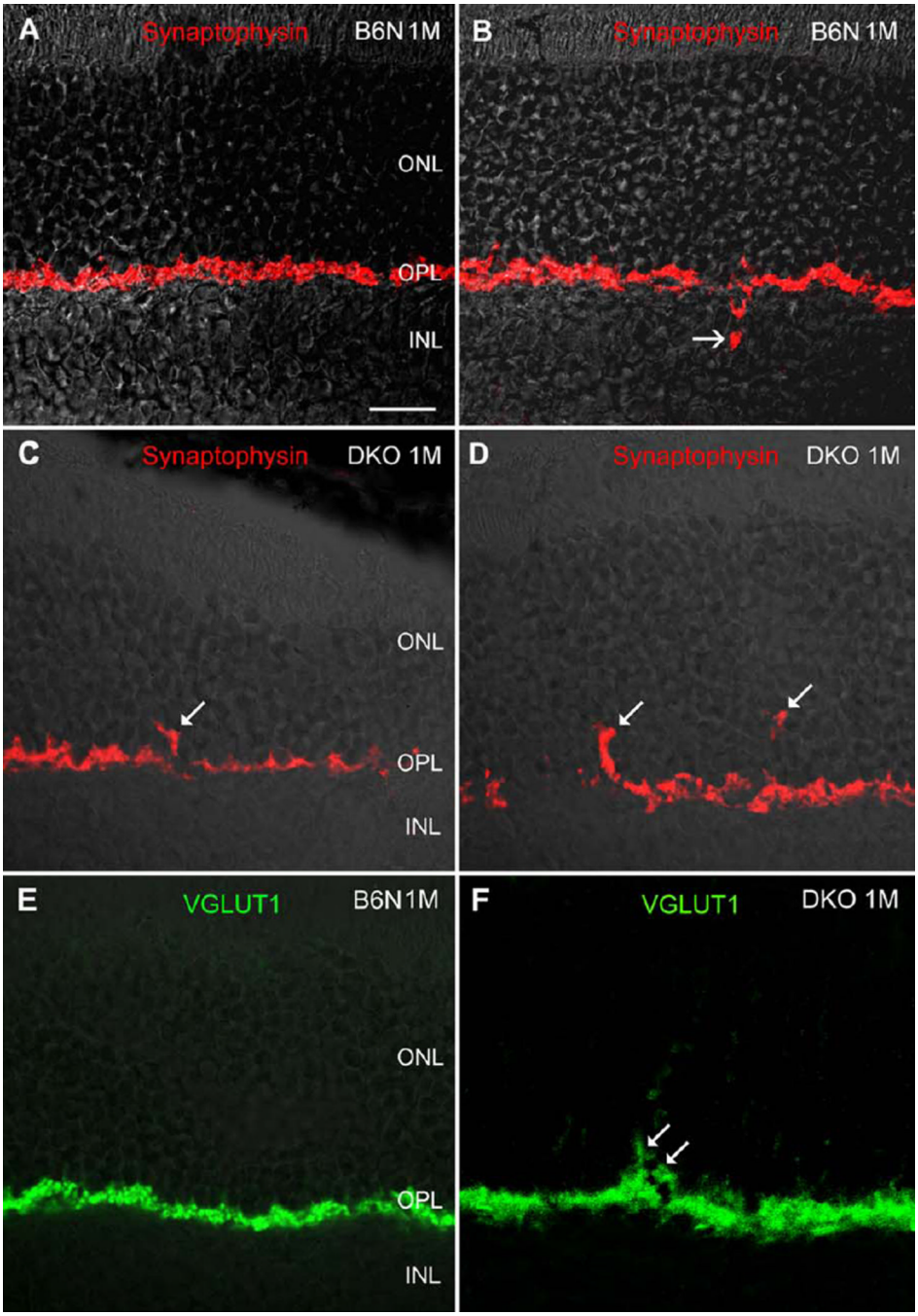

Fig. 4.

Confocal images showing synaptophysin and VGLUT1 IR immunoreactivity on the vertical sections in the B6N and the DKO mice. **A, B**: Intense synaptophysin IR is always evident in the OPL, but occasionally detectable in the INL (B, arrow) in the B6N mice, indicating inward protrusion of photoreceptor terminals. **C, D**: In DKO mice, synaptophysin labeled punctas are found in the ONL (arrows). **E, F**: Similarly, VGLUT1 labeling is found in the OPL in the B6N mice, whereas in the DKO retina VGLUT1 puncta is readily visible in the ONL (F, arrow). Scale bar: 20 μm for A–F.

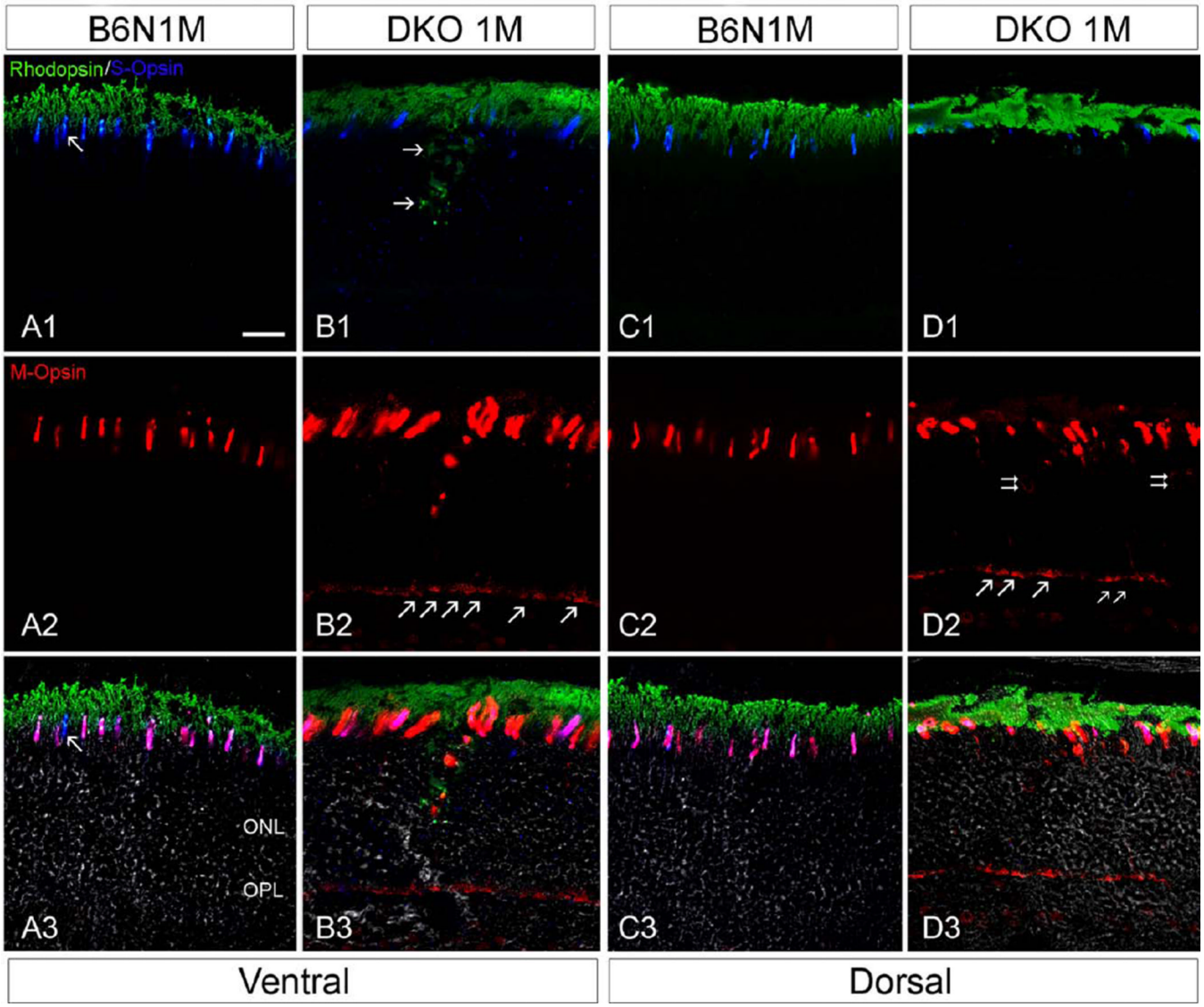

Fig. 5.

Confocal images showing triple-labeling of cone M- and S-opsin and rod rhodopsin IR on the vertical sections in the B6N and the DKO mice. **A, C**: In the B6N mice, the co-expression of S- and M-opsin is evident in cone OS, either ventral (A1–3) or dorsal (C1–3), whereas a rare cone that appears to express S opsin only (arrows). **B, D**: In the DKO mice, S-opsin appear dramatically decreased, resulting in reduced co-expression of S- and M-opsin (B1–3, D1–3). Furthermore, S-opsin in ventral region is more extensively mislocalized throughout the IS, ONL, OPL, and even INL (B1), whereas those in dorsal region are less mislocalized (D1). M-opsin is widely mislocalized in cytoplasmic membranes of soma (D2, double arrows) and axons (B2, D2), particularly in cone pedicles (arrows in B2, D2). Rhodopsin mislocalization is evident in the IS and INL of the ventral region but rarely in the soma, axons and OPL in DKO mice (C1–3), whereas those in the dorsal region appear normal (D1). Scale bar: 20 μm for all.

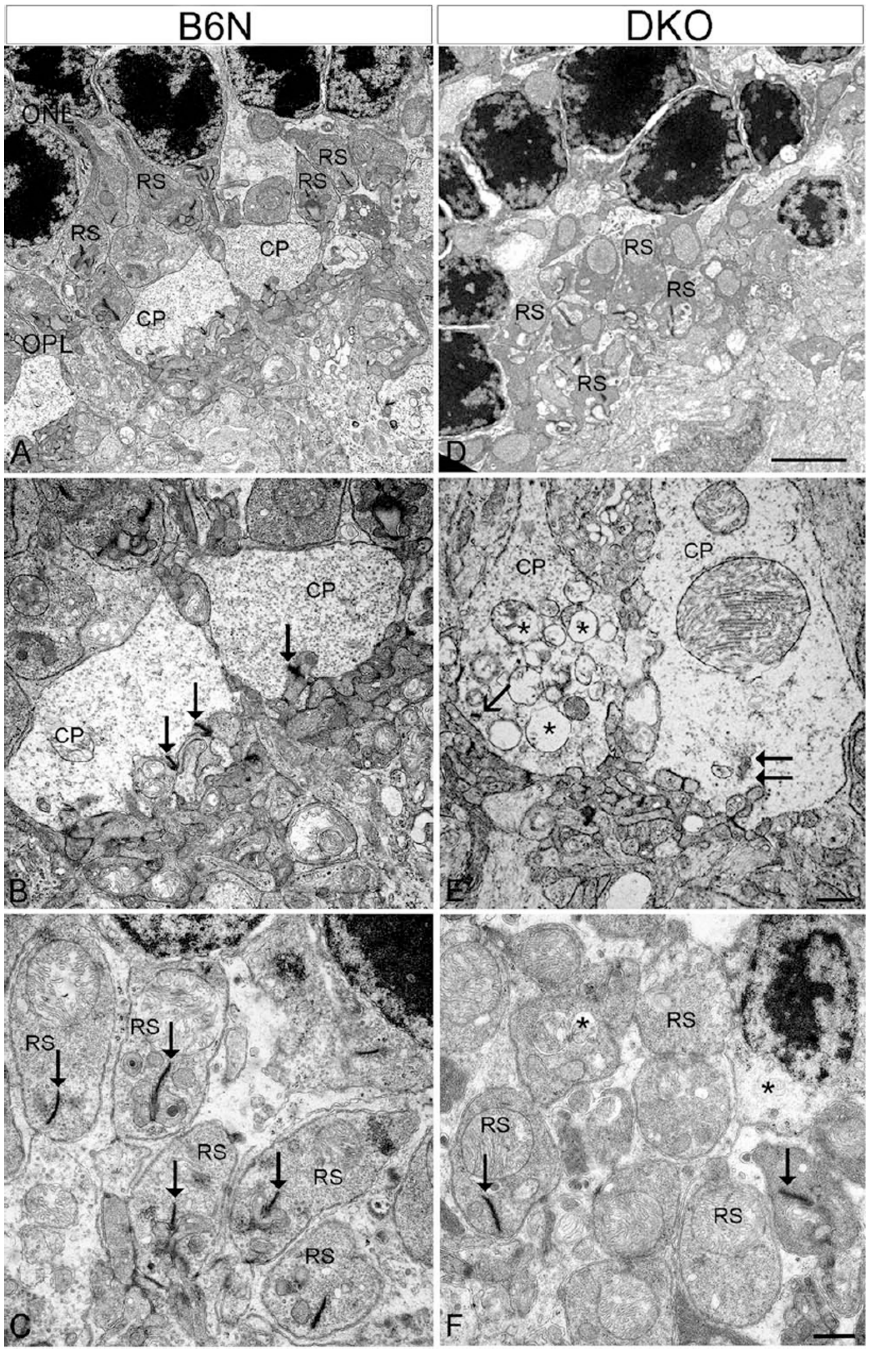

Fig. 6.

EM micrographs showing the degeneration of photoreceptor terminals in DKO mice compared with B6N mice. **A–C**: In the B6N mice, the cone pedicles (CP) and rod spherules (RS) are organized regularly in the OPL (A), in which CP contains various synaptic ribbons (B, arrows) and RS has only one ribbon (C, arrows). **D–F**: The DKO mice show highly disorganized photoreceptor terminals in the OPL (D). At high power, DKO retinas show marked reduction of synaptic ribbons and shallower or flattened invaginations in both CP (E) and RS (F). Some CP contain short and “floating” ribbons (E, arrows), but numerous vacuoles (E, asterisks). Synaptic vesicles appear loosely packed in these two degenerate CP

(E). However, RS had less vacuole (F) compared with CP. Scale bar: 2 μm for A and D, 500 nm for B, C and E, F.

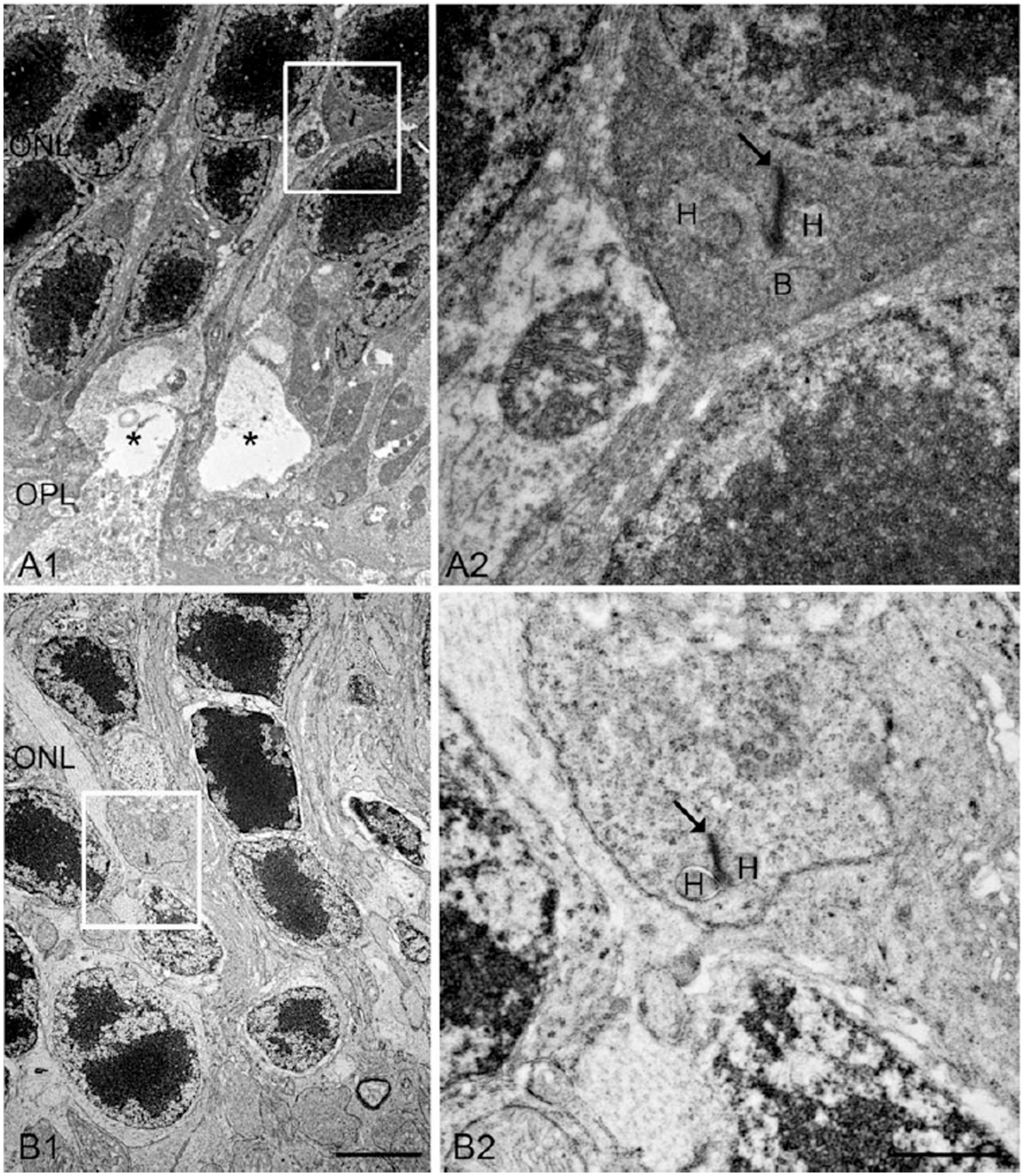

Fig. 7.

EM micrographs showing ectopic rod synapses in the ONL in the DKO mice. **A**: A rod spherule retracts into the ONL (A1, square), where a new ectopic rod synapse is illustrated at high power image (A2). A similar example is shown respectively on **B1** and B2, however, only two HCs are observed in this case. Arrows, ribbons; asterisks, vacuoles; H, HC; B, RBC. Scale bar: 2 μm for A1 and B1, 500 nm for A2 and B2.

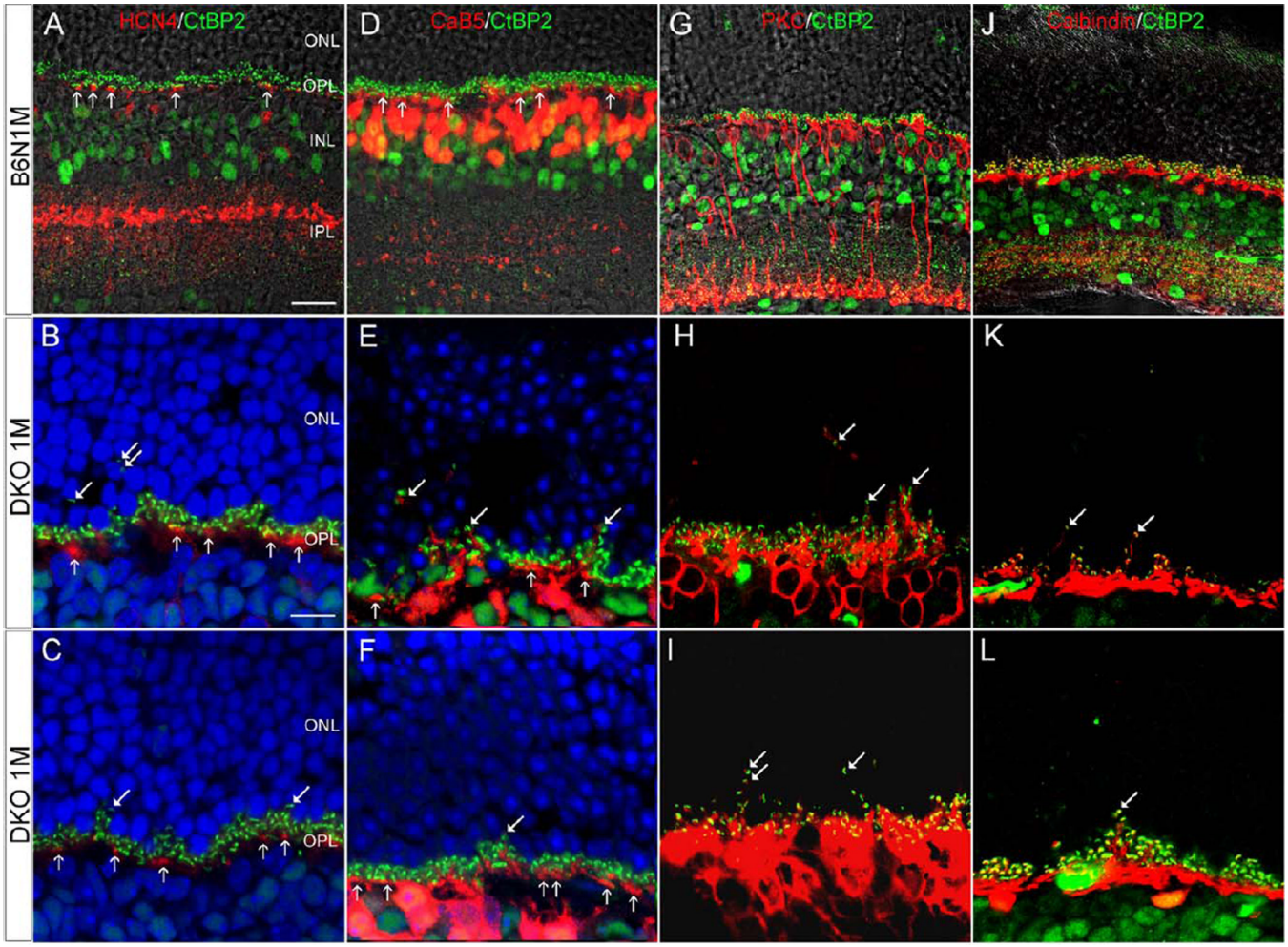

Fig. 8.

Confocal images showing postsynaptic neuron on the vertical sections in the B6N and the DKO mice. **A–C**: HCN4 IR shows that OFF-CBC dendrites are exclusively in the OPL (vertical arrows) in B6N (A) and DKO mice (B, C), though CtBP2 punctas are visible in the ONL in DKO mice (arrows in B, C). **D–F**: CaB5 labeled dendrites are exclusively in the OPL of B6N mice (vertical arrows in D) whereas a few dendrites are evident in the ONL in DKO mice (arrows in E, F). **G–L**: PKC-labeled RBC dendrites (G) and Calbindin-labeled HC processes (J) are restricted in the OPL of B6N retinas. In DKO mice, however, fine PKC-labeled RBC dendrites and Calbindin-labeled HC processes are extended into the ONL, which demonstrate a close association with CtBP2-labeled synaptic ribbons (arrows in H, I, K, and L). Scale bar: 20 μm for A, D, G and J; 10 μm for B and others.

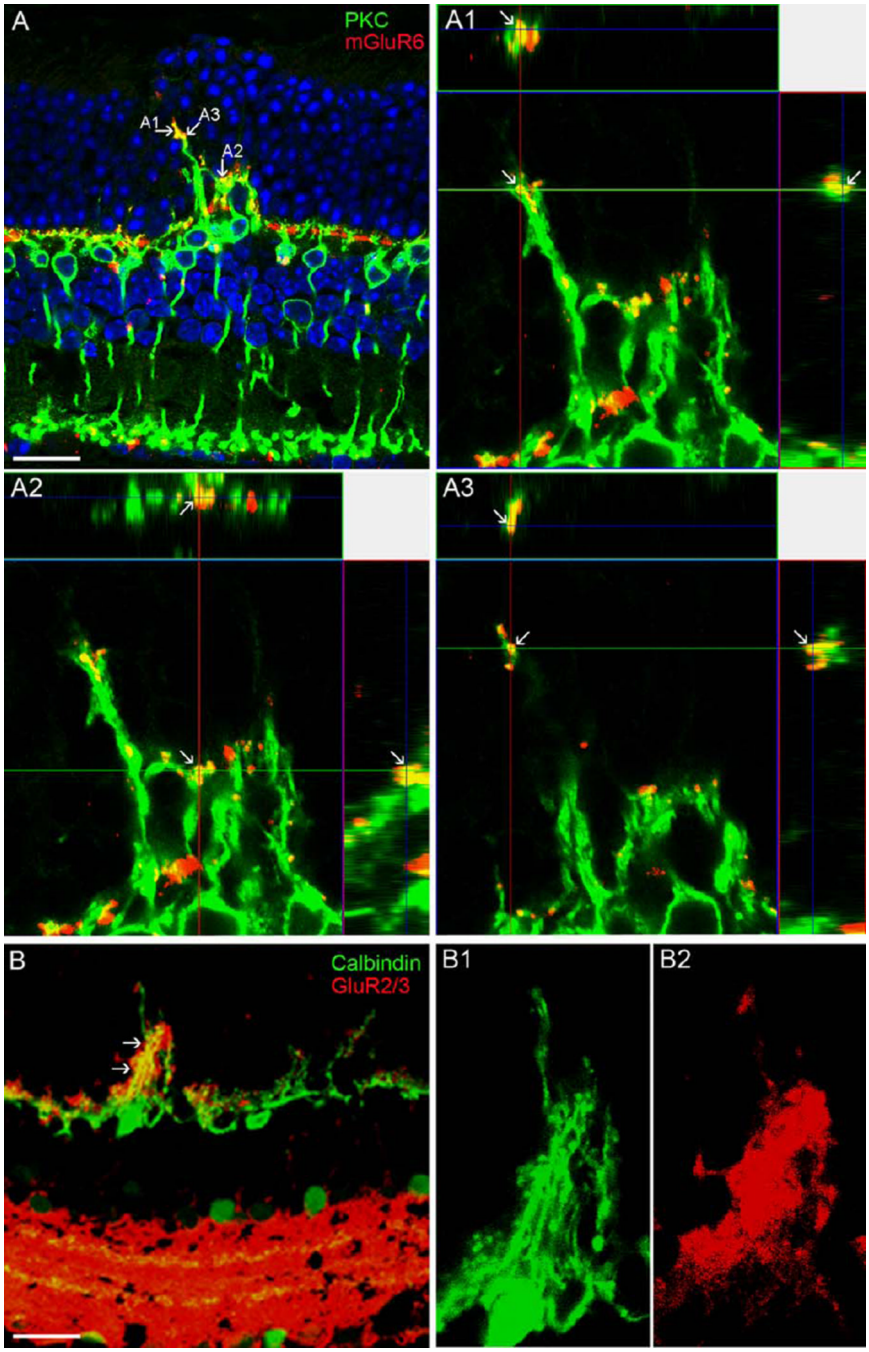

Fig. 9.

Confocal images showing glutamate receptor labeling in the DKO mice. **A**: mGluR6 puncta are ectopically expressed in the ONL and colocalized with the sprouting of RBC dendrites labeled by PKC (arrows). A1-A3 illustrate three points shown in A through *xy*, *xz*, and *yz* planes (arrows), confirming a colocalization of two proteins. **B**: Similarly, GluR2/3 puncta are ectopically expressed in the ONL and colocalized with the sprouting of HC processes labeled by Calbindin (arrows). High magnified images are illustrated in Bl and B2. Scale bar: 20 μm.

TABLE I

List of primary antibodies used for immunofluorescence

Antibody	Cell type/target	Dilution	Source
Mouse anti-CtBP2	Synaptic ribbons	1:100	BD Transduction Lab
Mouse anti-synaptophysin	Synaptic vesicles	1:500	Millipore
Rabbit anti-L/M opsin	Red/green cone outsegments	1:1000	Millipore
Goat anti-S opsin	Blue cone outsegments	1:100	Santa Cruz Biotech
Mouse anti-Rhodopsin	Rod outsegments	1:100	Millipore
Mouse anti-PKC	Rod bipolar cells	1:100	Sigma
Rabbit anti-PKC	Rod bipolar cells	1:10000	Santa Cruz Biotech
Rabbit anti-HCN4	OFF cone bipolar cells	1:1500	Alomone Lab
Rabbit anti-CaB5	ON cone bipolar cells	1:1000	F Haeseleer, Seattle,WA
Mouse anti-Calbindin D28	Horizontal cells	1:200	Millipore
Sheep anti-mGluR6	On-bipolar cell dendritic tips	1:100	C. Morgans, Portland, OR
Mouse anti-GluR3	Horizontal cell processes	1:100	Millipore
Guinea pig anti-VGLUTl	Vesicular glutamate transporter 1	1:20000	Millipore

TABLE II

Distribution of the photoreceptor terminals of C57BL/ 6N rd8 and DKO rd8 mice

	C57BIV6N *rd8* No. (%)	DKO *rd8* No. (%)	*P*
Total terminals	1497[a]	1427[a]	
Cone terminals	109 (8)	27(2)	
Rod terminals	1388 (92)	1400 (98)	<0.01
Cone terminals			
With ribbon	90 (83)	16 (59)	
Without ribbon	19 (17)	11(41)	<0.01
Rod terminals			
With ribbon	946 (68)	588 (42)	
Without ribbon	442 (32)	812 (58)	<0.01

[a]The samples were collected from EM sections processed from four eyes of each strain.